Design and Analysis of a Totally Decoupled Flexure-Based XY Parallel Micromanipulator

Yangmin Li, *Senior Member, IEEE*, and Qingsong Xu

***Abstract*—In this paper, a concept of totally decoupling is proposed for the design of a flexure parallel micromanipulator with both input and output decoupling. Based on flexure hinges, the design procedure for an XY totally decoupled parallel stage (TDPS) is presented, which is featured with decoupled actuation and decoupled output motion as well. By employing (double) compound parallelogram flexures and a compact displacement amplifier, a class of novel XY TDPS with simple and symmetric structures are enumerated, and one example is chosen for further analysis. The kinematic and dynamic modeling of the manipulator are conducted by resorting to compliance and stiffness analysis based on the matrix method, which are validated by finite-element analysis (FEA). In view of predefined performance constraints, the dimension optimization is carried out by means of particle swarm optimization, and a prototype of the optimized stage is fabricated for performance tests. Both FEA and experimental studies well validate the decoupling property of the XY stage that is expected to be adopted into micro-/nanoscale manipulations.**

***Index Terms*—Dynamics, kinematics, mechanism design, micro-/nanorobots, parallel robots.**

I. Introduction

NOWADAYS, compliant positioning stages with ultrahigh precision play more and more important roles in applications where a high-resolution motion over a microrange is expected in the cases of microelectromechanical system (MEMS) sensors and actuators, optical fiber alignment, biological cell manipulation, and scanning probe microscope. An XY translational stage is needed in an atomic force microscope (AFM) [1] for scanning of the probe over samples to get information such as surface profile of the scanned materials. A great number of compliant stages proposed for the pertinent applications can be found in the literature [2]–[7]. Compliant stages based on flexure hinges transmit motions by resorting to elastic deformation of the material [8]. The flexures instead of conventional mechanical joints endow a mechanism with several advantages including no backlash, no friction, vacuum compatibility, and easy to manufacture [9]. This paper is concentrated on the investigation of compliant XY manipulators due to their promising applications in micro-/nanofields. Some XY stages are commercially available from a number of companies including the PI, Thorlabs, etc. However, most commercial products adopt a stacked or nested structure with two 1-DOF positioning stages. The serial connection of two stages enables a simple control strategy since the X and Y translations can be controlled independently, which is at the expense of a high inertia, low natural frequency, and cumulative errors. To overcome such drawbacks, an XY stage with parallel architecture [10], [11] is a potential alternative. A parallel kinematic structure can be adopted in a flexure mechanism due to its contribution to high load-carrying capacity, high accuracy, low inertia, and compact size. Some XY stages with parallel kinematics are reported in the literature of [12]–[18], and some of them have been commercialized.

However, most of the proposed positioning stages have a coupled motion and stress stiffening effect. In compliant mechanisms, stress stiffening means the stiffening of a structure due to its stress state, which usually arises from overconstraint, and augments the transverse stiffness in the presence of axial stresses [19]. This phenomenon should be avoided since it brings amplified forces and reduced strokes to the structure, and accordingly causes nonlinearities to actuation [20]. Moreover, in situations where the stage is underactuated or the sensory feedback of the mobile platform (output platform of the stage) positions is not allowed, a decoupled XY stage with proper calibrations is preferred [21]. A decoupled stage usually means that one actuator produces only one axial output motion of the mobile platform. The term "decoupled" refers to the output decoupling of the stage. Nevertheless, input decoupling of compliant stages is seldom paid attention since it emphasizes on the isolation of actuation instead. When the stage is driven by one actuator, other actuators may suffer from undesired (such as bending) loads due to the movement of the mobile platform, or clearances may exist between other actuators and interfaces with the stage [22].Corresponding to output decoupling, the input decoupling can be defined as the isolation of actuation for a compliant stage [21].

In this paper, the idea of totally decoupling is extended from the aforementioned two decoupling concepts to design a compliant parallel micromanipulator. Hence, a totally decoupled parallel stage (TDPS) is defined as a compliant parallel positioning stage with both input and output decoupling. The design of a TDPS is a challenging work even for an XY stage. Among previous works dedicated to compliant XY parallel stages, the design of a totally decoupled one is pioneered in [21] and [23] using double parallelogram leaf flexures. The presented XY stages are directly driven by linear actuators without displacement amplifiers, which results in a stage workspace equal to the stroke of actuators. In case that the stroke is not satisfied, a displacement amplification device is a nice choice. However,

Manuscript received June 20, 2008; revised October 18, 2008. First published March 16, 2009; current version published June 5, 2009. This paper was recommended for publication by Associate Editor I. Bonev and Editor F. Park upon evaluation of the reviewers' comments. This work was supported in part by the Research Committee of the University of Macau under Grant RG-UL/07-08S/Y1/LYM/FST and in part by the Macao Science and Technology Development Fund under Grant 069/2005/A.

The authors are with the Faculty of Science and Technology, Department of Electromechanical Engineering, University of Macau, Macao, China (e-mail: ymli@umac.mo; qsxu@umac.mo).

Digital Object Identifier 10.1109/TRO.2009.2014130

additional amplifiers for those stages will complicate their structures even more. The main contribution of the current research is the integrated design of a class of XY TDPS with displacement amplifiers. Compared to previous XY stage in [21], which possesses a rotation-symmetric structure, the TDPS presented here is mirror-symmetric instead, which is superior to the former in terms of accuracy performance. Besides, with comparison to the mirror-symmetric XY stage evolved in [23], the architecture of the current stage is designed much simpler for the ease of manufacture from economical point of view. On the other hand, it is observed that the proposed XY TDPS is similar to the four prismatic–prismatic (PP) mechanism presented in [14], [17], and [18]. An insightful comparison reveals that the four outer P joints adopt double compound parallelogram flexures whereas the four inner P joints employ simple parallelogram flexures in the said mechanism. Thus, parasitic translations exist in the two working axes [14]. In contrast, the proposed stage possesses fully decoupled output motion without crosstalk between the two axes in theory since all the P joints are implemented with double compound parallelogram flexures.

In the remainder of the paper, the design and enumeration of an XY TDPS are presented in Section II, where one stage is proposed as an example for the subsequent studies. Based on the matrix method used in Section III, compliance and stiffness modeling of the stage are performed in Section IV, and kinematics and dynamics analyses are conducted in Section V, both with finite-element analysis (FEA) validations. Then, the optimal dimension design of the stage is carried out in Section VI by means of particle swarm optimization (PSO), and the performances of the resulted stage are tested by FEA in Section VII. Moreover, the stage is fabricated along with experiments conducted in Section VIII. Finally, some concluding remarks are summarized in Section IX.

II. Design and Enumeration of an XY TDPS

A. Design of a Decoupled XY Compliant Stage

In rigid-body mechanism, a planar parallel manipulator with two translational motions can be synthesized via the screw theory [24], [25] or Lie groups approach [26], [27], etc. For example, the structure can be designed as 5R, PRRRP, RPRPR [11], [28], 2-PPa [29], and 2-RPa, etc., where the notations of R, P, and Pa denote the revolute, prismatic, and parallelogram joints, respectively. In order to design a decoupled XY compliant stage, an overconstrained 2-PP parallel mechanism is employed due to its simple structure, as shown in Fig. 1, where two configurations are produced according to the inside or outside assembly of the mobile platform. Although a rigid-body 2-PP parallel manipulator cannot work properly without joint clearances, a 2-PP compliant mechanism can still operate well due to the compliances of flexure elements. With an orthogonal arrangement of the two PP limbs, the X and Y translations of a 2-PP mechanism will be decoupled as long as ideal P joints are used. Furthermore, by adopting compound parallelogram flexures, four typical P joints without stiffening and buckling are sketched in Fig. 2, where the ideal translations of the primary stages without cross-axis errors are enabled by assigning the same length (l) to the four limbs. Based on these basic joints, a number of flexure XY parallel stages can be enumerated.

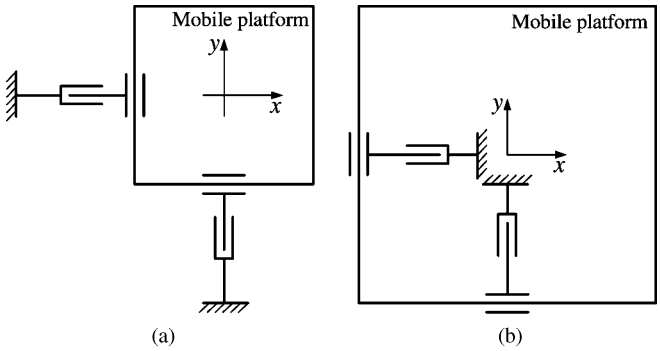

Fig. 1. Schematic diagram of a 2-PP parallel mechanism.

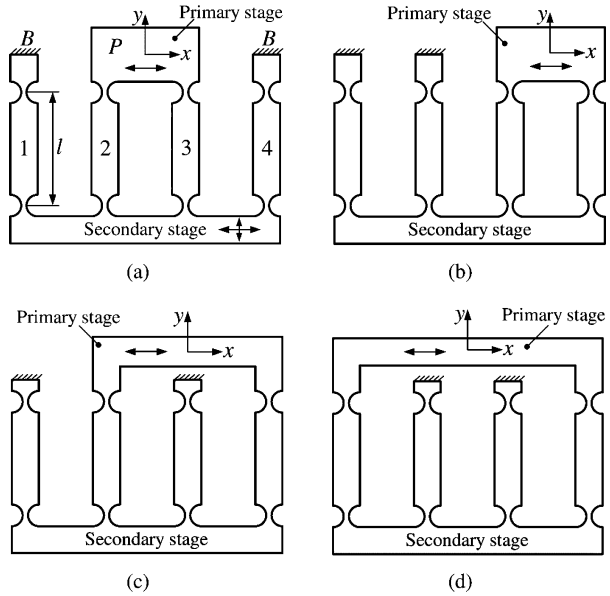

Fig. 2. Typical P joints employing compound parallelogram flexures.

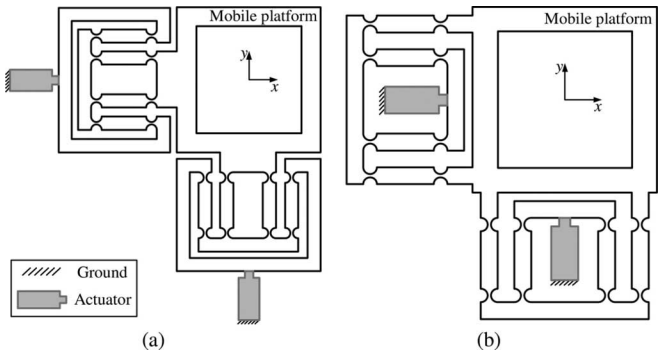

Fig. 3. Conceptual design of an XY stage with decoupled motion.

For example, by adopting the flexure P joints, as shown in Fig. 2(a) and (d), conceptual designs of a decoupled XY stage are proposed in Fig. 3(a) and (b), respectively, where the scheme in Fig. 1(a) is used as an illustration. Once actuated by two linear actuators that are mounted by rigid connections at the interfaces, the output translations of the stage are decoupled. However,

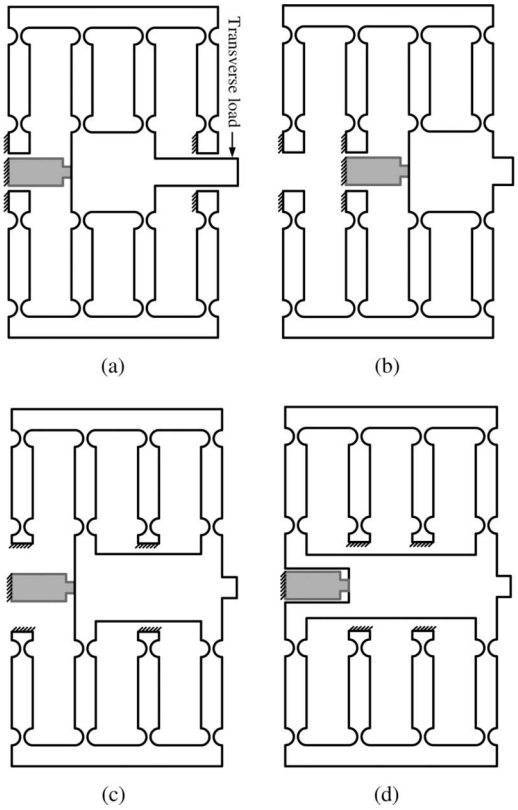

Fig. 4. Double compound parallelogram flexure stages with large transverse stiffness.

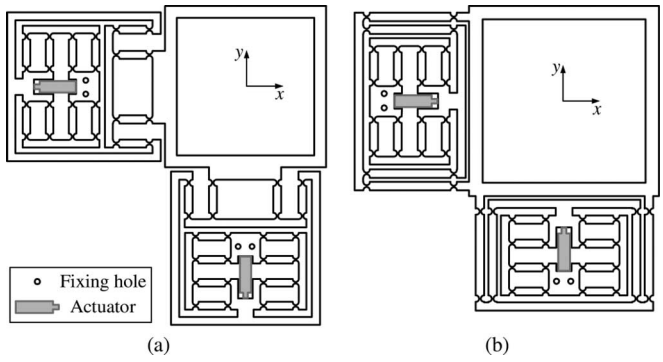

Fig. 5. XY TDPS without displacement amplifier.

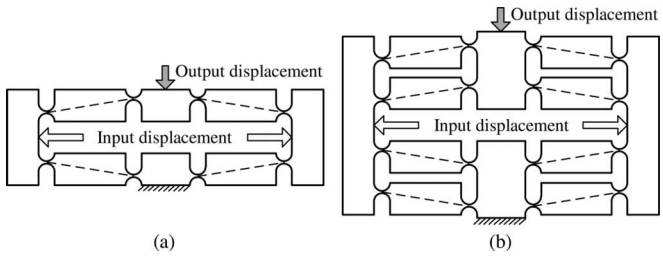

Fig. 6. (a) Original displacement amplifier and (b) an improved displacement amplifier with high transverse stiffness.

transverse loads or bending moments are exerted on the mounted actuators at the same time, which will cause damages to linear actuators such as piezoelectric actuator (PZT). This is one of the reasons why actuation decoupling is desirable in an XY stage. In order to implement actuator decoupling, an additional P joint can be added between each actuator and the stage as a decoupler or bearing, whose roles are to transmit axial force of actuator, and prevent the actuator from suffering undesired lateral motions and loads as well.

It follows that the bearing should possess both a high compliance in its working direction and a high stiffness in transverse direction at the same time. In this sense, the transverse stiffness of the P joints, as shown in Fig. 2, may not be sufficient, which can be enhanced by combining two identical P joints in parallel to form a double compound parallelogram flexures, as illustrated in Fig. 4. Each of the four pure translational stages can be adopted as a bearing to achieve the goal of input decoupling. For instance, by employing the flexure, as described in Fig. 4(b), two totally decoupled XY parallel stages are designed, as shown in Fig. 5, from which a mirror-symmetric (or double symmetric) structure with respect to both x- and y-axis can be generated by adding two auxiliary limbs to each stage.

B. Design of a TDPS With Displacement Amplifier

PZT is widely used in precision instruments due to its major advantages of large blocking force, high stiffness, fast response, and compact size. Comparing with other types of linear actuators, the main drawback of PZT lies in its small travel stroke. If the stroke of the adopted PZT cannot meet application requirements, a proper amplification mechanism will be exploited to suit the needs.

As far as the designed XY stage with piezoactuation is concerned, once a large-stage workspace is demanded, the stroke of the PZT can be amplified by adopting any types of lever mechanism connecting to the decoupler. Even so, in order to design an XY stage with a compact and simple structure, and to fully exploit the large blocking force and stiffness of PZT, the displacement amplification device, as illustrated in Fig. 6(a), is employed. It has been shown in [30] and [31] that this type of amplifier possesses a number of merits including a compact size and large amplification ratio. However, this amplifier has a relatively low transverse stiffness at its output end and cannot guarantee a linear output motion. For the sake of enhancing the transverse stiffness while maintaining the same shape and size of flexure hinges, the amplifier is improved, as shown in Fig. 6(b), which acts as a decoupler and has the roles of both linear motion guide and displacement amplification [18]. By replacing the bearing between PZT and XY stage with the proposed displacement amplifier, one resulted XY TDPS is shown in Fig. 7 as an illustration, where a symmetric structure is adopted due to its contribution to performance improvement of the stage.

Since the bearings, as shown in Fig. 4, are sufficient to isolate actuators, the employed displacement amplifier is a redundant design to provide actuator decoupling. One limitation of the amplifier lies in the movable mass of actuator, which arises from the fact that the entire actuator translates $d/2$ along a direction vertical to actuation axis once the amplifier is driven to produce an output displacement of d. The movement of actuator should

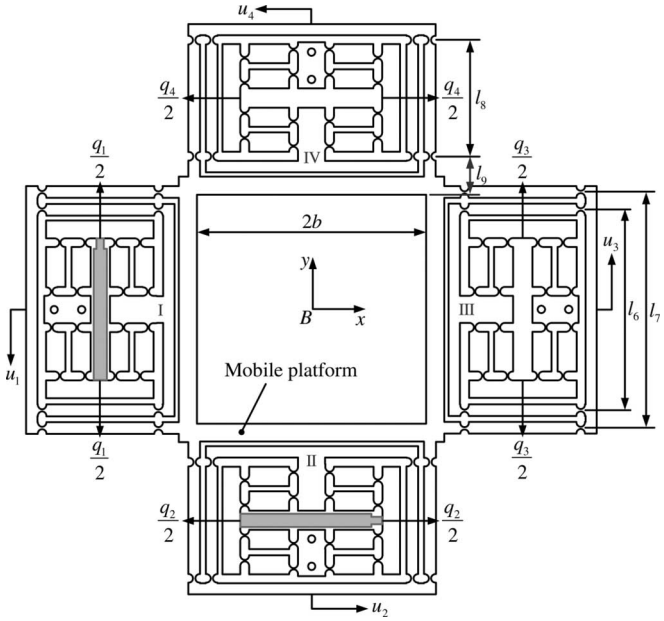

Fig. 7. Symmetric XY TDPS with displacement amplifier.

be considered in physical modeling of the stage for a precision control purpose, especially as the value of $d/2$ reaches to a macroscale.

Note that any other types of flexure hinges (e.g., elliptical, right angle, and corner-filleted hinges) can be adopted in the compliant stage design, although only the right circular hinge is employed here. As an example, the modeling and evaluation of the XY stage, as shown in Fig. 7, will be conducted in the following discussions.

III. Compliance Modeling of Flexure Mechanisms Based on Matrix Method

The compliant mechanisms can be modeled through various approaches [32]. The mostly used techniques are based upon simplifications such as the well-known pseudorigid body (PRB) method [33]. However, PRB model cannot be utilized for a complete compliance/stiffness analysis since it only considers the compliances of flexures in their working directions. To establish a full kinematic or compliance/stiffness model of a compliant mechanism, nonlinear modeling approach in view of deformations (in terms of bending, torsion, and tensile/compression) of each component of the mechanism can be executed. However, the fully modeling is not a straightforward work since numerous integral operations are involved. As a compromise, the lumped model of a flexure with the consideration of 6-D (or concerned) compliance in space can be employed. Such a lumped model can be derived effectively by the matrix method under the assumption of Hooke's law for the material, since matrix operations can be easily conducted with higher calculation efficiency [34]–[37]. In what follows, the matrix-based compliance/stiffness modeling is demonstrated and confirmed on the proposed XY TDPS.

It is known that a 6×6 compliance (or stiffness) matrix model for each flexure element can be expressed in its local coordinate system. The compliance matrix for a right circular flexure hinge with the coordinate frame assigned in Fig. 8 can be written as

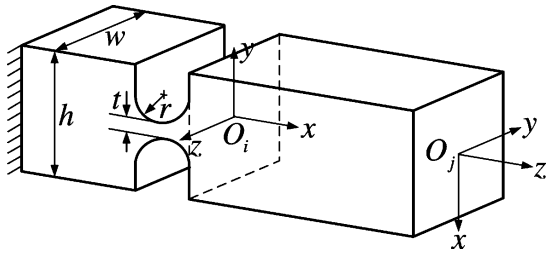

Fig. 8. Parameters of a flexure hinge with coordinates.

$$\mathbf{C}_h = \left[\begin{array}{cc|ccc|c} \frac{\Delta x}{\Delta F_x} & 0 & 0 & 0 & 0 & 0 \\ 0 & \frac{\Delta y}{\Delta F_y} & 0 & 0 & 0 & \frac{\Delta y}{\Delta M_z} \\ \hline 0 & 0 & \frac{\Delta z}{\Delta F_z} & 0 & \frac{\Delta z}{\Delta M_y} & 0 \\ 0 & 0 & 0 & \frac{\Delta \theta_x}{\Delta M_x} & 0 & 0 \\ 0 & 0 & \frac{\Delta \theta_y}{\Delta F_z} & 0 & \frac{\Delta \theta_y}{\Delta M_y} & 0 \\ \hline 0 & \frac{\Delta \theta_z}{\Delta F_y} & 0 & 0 & 0 & \frac{\Delta \theta_z}{\Delta M_z} \end{array}\right] \quad (1)$$

where the compliance factors in the matrix have been derived in several references, and the equations with best accuracy, as reviewed in [38], are adopted in this paper. The $\mathbf{C}_h$ represents the compliance of free end O_i with respect to the other fixed end. It has been shown in [39] that the compliance matrix for a flexure hinge can be made diagonal by a proper choice of local coordinate system. For a planar XY stage investigated in this paper, the most important compliance factors $\mathbf{C}_h(1,1)$, $\mathbf{C}_h(2,2)$, and $\mathbf{C}_h(6,6)$ already construct a diagonal form, so the effort toward diagonalizing the whole compliance matrix is saved.

Additionally, referring to Fig. 8, the local compliance of the hinge is defined as $\mathbf{C}_i^0 = \mathbf{C}_h$, where the upper-right superscript describes the coordinate with respect to which the compliance is described throughout this paper, and "0" indicates the ground that will be omitted for the clarity of representation. The compliance $\mathbf{C}_i$ can be transferred into another frame O_j by

$$\mathbf{C}_i^j = \mathbf{T}_i^j \mathbf{C}_i (\mathbf{T}_i^j)^T \quad (2)$$

where the transformation matrix takes on the following form:

$$\mathbf{T}_i^j = \begin{bmatrix} \mathbf{R}_i^j & \mathbf{S}(\mathbf{r}_i^j)\mathbf{R}_i^j \\ \mathbf{0} & \mathbf{R}_i^j \end{bmatrix} \quad (3)$$

where $\mathbf{R}_i^j$ is the rotation matrix of coordinate O_i with respect to O_j, $\mathbf{r}_i^j$ is the position vector of point O_i expressed in reference frame O_j, and $\mathbf{S}(\mathbf{r})$ represents the skew-symmetric operator for

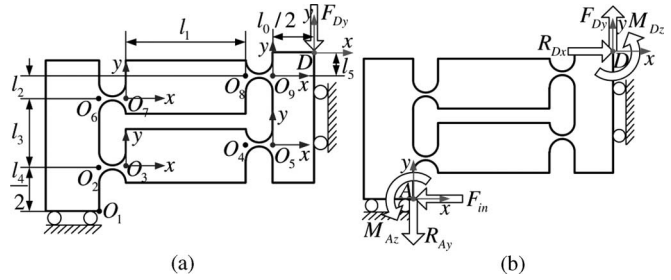

Fig. 9. Parameters and coordinates for one quarter of the displacement amplifier.

a vector $\mathbf{r} = [r_x \;\; r_y \;\; r_z]^T$ with the notation

$$\mathbf{S}(\mathbf{r}) = \begin{bmatrix} 0 & -r_z & r_y \\ r_z & 0 & -r_x \\ -r_y & r_x & 0 \end{bmatrix}. \tag{4}$$

Generally, a flexure mechanism consists of n individual flexure elements connected in serial or parallel manners. In order to obtain the compliance model of the entire mechanism, the local compliances need to be transformed to a common (global) frame chosen to describe the mechanism. Then, compliances connected in serial and stiffnesses connected in parallel can be, respectively, added together to generate the entire model of the flexure mechanism.

IV. Compliance and Stiffness Modeling of the XY Stage

The output compliance $\mathbf{C}_B$ is defined as the compliance of point B (where the external force $\mathbf{F}_B$ is exerted) with respect to the ground, which reflects the manipulation accuracy of the manipulator with external forces exerted at the end-effector. On the contrary, the input stiffness $\mathbf{K}_A$ is defined as the stiffness of input end A (where the input force $\mathbf{F}_A$ is applied) with respect to the ground, which should not exceed the minimum output stiffness of the adopted actuator. Note that the compliance and stiffness models for the mechanism of the stage are established in this research without considering the compliances of actuators. To obtain a static model of the mechanism with the consideration of piezoactuators, a methodology, as proposed in [40], can be employed to establish the relationship between the applied voltage and output displacement of the stage.

A. Output Compliance Modeling

1) Output Compliance of One Displacement Amplifier: Due to the double symmetric property, one quarter of the amplifier is picked out, as shown in Fig. 9(a), for the purpose of analysis. The output compliance $\mathbf{C}_D^1$ is defined as the compliance of point D with respect to the input end O_1.

Due to serial connections, the compliances of D with respect to O_2 and O_6 can be, respectively, derived as

$$\mathbf{C}_D^2 = \mathbf{T}_3^D \mathbf{C}_3 (\mathbf{T}_3^D)^T + \mathbf{T}_5^D \mathbf{C}_5 (\mathbf{T}_5^D)^T \tag{5}$$

$$\mathbf{C}_D^6 = \mathbf{T}_7^D \mathbf{C}_7 (\mathbf{T}_7^D)^T + \mathbf{T}_9^D \mathbf{C}_9 (\mathbf{T}_9^D)^T \tag{6}$$

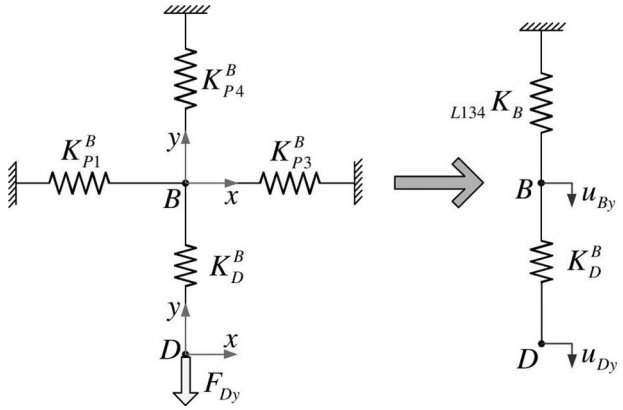

Fig. 10. Stiffness model of the XY stage with one limb actuated.

where the local compliances $\mathbf{C}_i = \mathbf{C}_h$ (for $i = 3, 5, 7$, and 9) and $\mathbf{T}_i^D$ are the transformation matrices.

In view of the parallel connection between the two chains DO_5O_2 and DO_9O_6, compliance $\mathbf{C}_D^1$ can be obtained as

$$\begin{aligned} \mathbf{C}_D^1 &= (\mathbf{K}_D^1)^{-1} = (\mathbf{K}_D^2 + \mathbf{K}_D^6)^{-1} \\ &= [(\mathbf{C}_D^2)^{-1} + (\mathbf{C}_D^6)^{-1}]^{-1}. \end{aligned} \tag{7}$$

Assign ${}_{\mathrm{tl}}\mathbf{C}_D$ as the output compliance of top-left part of the amplifier with respect to the ground, then ${}_{\mathrm{tl}}\mathbf{C}_D = \mathbf{C}_D^1$, where the lower-left subscript records a certain part of the concerned object. Due to the top–down symmetry of the amplifier, the compliance of the left section can be written as

$${}_l\mathbf{C}_D = {}_{\mathrm{tl}}\mathbf{C}_D + \mathbf{T}_d^t ({}_{\mathrm{tl}}\mathbf{C}_D)(\mathbf{T}_d^t)^T \tag{8}$$

with the transformation matrix transferring from the down to the top section

$$\mathbf{T}_d^t = \begin{bmatrix} \mathbf{R}_x(\pi) & \mathbf{0} \\ \mathbf{0} & \mathbf{R}_x(\pi) \end{bmatrix}. \tag{9}$$

Then, in view of the left–right symmetry, the compliance of the whole amplifier can be generated as

$$\mathbf{C}_D = (\mathbf{K}_D)^{-1} = [({}_l\mathbf{C}_D)^{-1} + (\mathbf{T}_r^l)^{-T} ({}_l\mathbf{C}_D)^{-1} (\mathbf{T}_r^l)^{-1}]^{-1} \tag{10}$$

where the transformation matrix from the right to the left section can be written as

$$\mathbf{T}_r^l = \begin{bmatrix} \mathbf{R}_y(\pi) & \mathbf{0} \\ \mathbf{0} & \mathbf{R}_y(\pi) \end{bmatrix}. \tag{11}$$

2) Output Compliance of the XY Stage: The XY stage consists of four individual limbs connected at the center point B in parallel. For each limb, the compliance $\mathbf{C}_{Bi}$ at point B can be derived by taking into account that the decoupler is connected to the primary stage of P joint (consisting of two parallel chains) in serial. Then, the output compliance $\mathbf{C}_B$ of the XY stage can be obtained by the summation of stiffnesses for the four limbs in the reference frame B.

B. Input Stiffness Modeling

Once the amplifier 2 is connected to the limb of the XY stage at point D as a decoupler, it will tolerate the force applied by the

remainder of the stage at the interface D. Excluding the amplifier in limb 2, the stiffness model of the stage is graphically depicted in Fig. 10, which interprets that the three parallel limbs (1, 3, and 4) are connected at the center point B, and then connected to point D through limb 2 whose compliances come from the P joint consisting of two parallel chains between B and D. The compliance of the XY stage without amplifier 2 can be obtained as follows:

$$\mathbf{C}_D = \mathbf{C}_D^B + \mathbf{T}_B^D ({}_{L134}\mathbf{K}_B)^{-1} (\mathbf{T}_B^D)^T. \tag{12}$$

Moreover, the free body diagram of one quarter of amplifier 2 is shown in Fig. 9(b), where the load $\mathbf{F}_{Dy}$ denotes the force along the y-direction applied by the XY stage excluding the amplifier which is actuated by a force $\mathbf{F}_{\rm in}$. Let $\mathbf{C}_A^D$ denote the compliance of input end A with respect to output end D, then $\mathbf{C}_A^D = \mathbf{C}_1^D$, which can be derived by the same way as in (7).

Assume that the output end D is fixed. In view of the force–deflection relationships at the input end, we can generate the following equations:

$$u_{\rm in} = c_{11} F_{\rm in} + c_{12} F_{Dy} + c_{16} M_{Az} \tag{13}$$

$$u_{Ay} = c_{21} F_{\rm in} + c_{22} F_{Dy} + c_{26} M_{Az} \tag{14}$$

$$\theta_{Az} = c_{61} F_{\rm in} + c_{62} F_{Dy} + c_{66} M_{Az} = 0 \tag{15}$$

where c_{ij} (for $i,\ j = 1, 2,$ and 6) are compliance factors in the ith row and jth column of the matrix $\mathbf{C}_A^D$. The four unknowns $u_{\rm in}$, u_{Ay}, F_{Dy}, and M_{Az} can be derived in terms of $F_{\rm in}$ from (13), (14), and (15) along with another equation, which can be obtained by taking into account the relationship between the load and deflection along the y-direction

$$u_{Ay} = -d_{22} F_{Dy} \tag{16}$$

where the parameter $d_{22} = \mathbf{C}_D(2,2)$ is a compliance factor of the matrix $\mathbf{C}_D$, and the negative sign indicates the opposite directions of the force F_{Dy} and deflection u_{Ay} at the input end A. In sequence, a necessary calculation allows the derivation of the input compliance for the XY stage

$$C_{\rm in} = \frac{u_{\rm in}}{F_{\rm in}} = c_{11} - \frac{c_{16} c_{61}}{c_{66}} - \left(c_{12} - \frac{c_{16} c_{62}}{c_{66}} \right) \frac{c_{21} c_{66} - c_{26} c_{61}}{c_{22} c_{66} - c_{26} c_{62} + d_{22} c_{66}} \tag{17}$$

from which, the input stiffness value $K_{\rm in} = 1/C_{\rm in}$ can be derived.

Accordingly, the output motion u_{Ay} can be obtained as a function of the input displacement $u_{\rm in}$

$$u_{Ay} = A_a\, u_{\rm in} = \frac{d_{22} (c_{21} c_{66} - c_{26} c_{61})\, u_{\rm in}}{(c_{22} c_{66} - c_{26} c_{62} + d_{22} c_{66})\, C_{\rm in}} \tag{18}$$

where A_a denotes the amplification ratio for the amplifier.

C. Stage Amplification Ratio Determination

With reference to Fig. 10, one can observe that when the stage is driven by the input motion $u_{\rm in}$, the displacement of point D along the y-direction is u_{Dy} ($u_{Dy} = u_{Ay}$). In view of the identical force along the y-direction in positions D and B, the output displacement at the mobile platform center B can be determined as

$$u_{By} = \frac{b_{22}}{d_{22}} u_{Dy} \tag{19}$$

where b_{22} denotes a compliance factor of compliance matrix ${}_{L134}\mathbf{C}_B$. Therefore, with the consideration of (18) and (19), the amplification ratio for the XY stage can be calculated as

$$A_s = \frac{u_{By}}{u_{\rm in}} = \frac{b_{22} (c_{21} c_{66} - c_{26} c_{61})}{(c_{22} c_{66} - c_{26} c_{62} + d_{22} c_{66})\, C_{\rm in}} \tag{20}$$

which partially determines the workspace size of the stage.

TABLE I
MAIN PARAMETERS OF AN XY STAGE

Architectural parameters (mm)							
r	t	h	w	l_0	l_1	l_2	l_3
3	0.5	8	12.7	8	10	1.5	10
l_4	l_5	l_6	l_7	l_8	l_9	b	
24	5	77.5	93.5	52	14.5	43.5	

Material parameters			
Young's modulus	Yield strength	Poisson's ratio	Density
71.7 GPa	503 MPa	0.33	2.81×10^3 kg/m^3

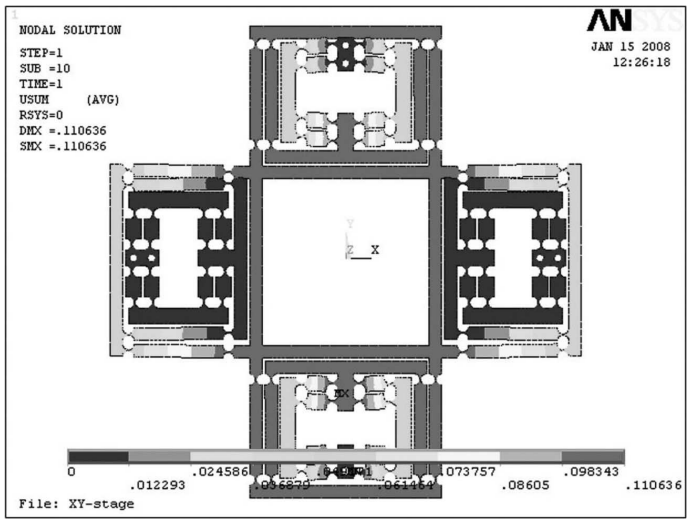

Fig. 11. Finite-element model of the XY stage.

D. Model Validation With FEA

The established models for the assessment of output compliance, input stiffness, and amplification ratio of the XY stage are validated by the FEA through ANSYS software. The architecture parameters of the stage are described in Table I where all the hinges are designed as identical dimensions, and the mesh model is created with the element PLANE82. When a displacement is applied at the input end of amplifier 2 (see Fig. 11), the corresponding input load and output motion of the mobile platform are obtained to determine the input stiffness and amplification ratio of the stage. Besides, the output compliance can be assessed by applying an external force to the mobile platform.

The stage performances evaluated by the derived models and FEA are elaborated in Table II. Taking FEA results as the benchmark, we can observe that the maximum deviation of the derived

TABLE II
KINETOSTATICS PERFORMANCES OF AN XY STAGE

Performance	Output compliance $\mathbf{C}_B(2,2)$ (μm/N)	Input stiffness (N/μm)	Amplification ratio
Matrix model	6.23	15.81	6.88
FEA	5.32	13.12	6.04
Deviation (%)	17.1	20.5	13.9

model from the FEA results is around 20%. The offset mainly comes from the accuracy of the adopted equations for the compliance factors and the neglect of compliances of the links between flexure hinges since these links are assumed to be rigid in the matrix model. To discover the effects of link compliances on the simulation results, an additional FEA is conducted with elastic modulus of the links set to be 100 times higher than that of flexure hinges. By this approach, the deformations of links are greatly reduced in ANSYS, and the differences between the stage performances obtained by matrix method and FEA are within 8%.

V. KINEMATICS AND DYNAMICS ANALYSIS

A. Mobility and Workspace Determination

For a stage with architecture parameters described in Table I, it can be derived that the output compliance matrix relates the planar deflections to the corresponding applied forces in such a manner

$$\begin{bmatrix} u_x \\ u_y \\ \theta_z \end{bmatrix} = \begin{bmatrix} 6.2\text{e}-6 & 0 & 0 \\ 0 & 6.2\text{e}-6 & 0 \\ 0 & 0 & 5.3\text{e}-4 \end{bmatrix} \begin{bmatrix} F_x \\ F_y \\ M_z \end{bmatrix}. \quad (21)$$

The diagonal form of the compliance (stiffness) matrix also indicates that the motion of the stage is decoupled.

In addition, as a planar mechanism, the number of DOFs for the stage can be calculated by the Grübler–Kutzbach criterion as three, which indicates that the designed flexure stage is nonoverconstrained, although it is based on a 2-PP mechanism. Besides, the passive rotational DOFs of the XY stage can only be exhibited when the mobile platform subjects to a moment around the z-axis.

With Q denoting the stroke of the adopted PZT, the workspace range of the XY stage can be derived as $A_sQ \times A_sQ$ as long as the stresses due to the rotations (σ_r) and axial loads (σ_t) of flexure hinges remain within the allowable stress σ_a of the material

$$\max\{\sigma^r, \sigma^t\} \le \sigma_a = \frac{\sigma_y}{n_a} \quad (22)$$

where $n_a \in (1, \infty)$ is an assigned safety factor and σ_y denotes the yield strength of the material.

1) Maximum Stress Subject to Rotation: Concerning a notch hinge bearing a bending moment around its rotation axis, the maximum angular displacement $\theta_{\max}$ arises when the maximum stress $\sigma^r_{\max}$, which occurs at the outermost surface of the thinnest portion of the hinge, reaches to the allowable stress σ_a.

Referring to [9], the relationship between the maximum stress and maximum rotation of the flexure hinge can be calculated by

$$\sigma^r_{\max} = \frac{E(1+\beta)^{9/20}}{\beta^2 f(\beta)}\,\theta_{\max} \quad (23)$$

where $\beta = t/2r$ is a dimensionless geometry factor with the valid range of $0 < \beta < 2.3$ and $f(\beta)$ is a dimensionless compliance factor defined in [9] as

$$f(\beta) = \frac{1}{2\beta+\beta^2}\left[\frac{3+4\beta+2\beta^2}{(1+\beta)(2\beta+\beta^2)} + \frac{6(1+\beta)}{(2\beta+\beta^2)^{3/2}}\tan^{-1}\left(\frac{2+\beta}{\beta}\right)^{1/2}\right]. \quad (24)$$

For each of the four limbs of the XY stage, the rotation angles of links associated with the amplifier and other links can be derived as

$$\phi_1 = \frac{(d_1/2)}{\sqrt{l_1^2+l_2^2}} \qquad \phi_2 = \frac{(x/2)}{l_8} \quad (25)$$

which arrive at the maximum values once the stage is actuated with a full stroke of the PZT. Under such a case, we have $d_1 = A_aQ$ and $x = A_sQ$.

Substituting the maximum rotation angles described by (25) into (23) allows the derivation of the relationships

$$\sqrt{l_1^2+l_2^2} \ge \frac{E(1+\beta)^{9/20} n_a A_a Q}{2\beta^2 f(\beta)\sigma_y} \quad (26a)$$

$$l_8 \ge \frac{E(1+\beta)^{9/20} n_a A_s Q}{2\beta^2 f(\beta)\sigma_y} \quad (26b)$$

which will provide a guideline for the design of the stage dimensions without the risk of inelastic deformations.

2) Maximum Tensile Stress Calculation: The maximum tensile stress subject to the axial load may occur on the thinnest portions of flexure hinges constructing the displacement amplifiers or other links of the stage, which can be determined by

$$\sigma_1^t = \frac{F_{\text{in}}}{S_{\min}} = \frac{K_{\text{in}}Q}{wt} \quad (27a)$$

$$\sigma_2^t = \frac{F_{Dy}}{S_{\min}} = \frac{(A_aQ/d_{22})}{wt} \quad (27b)$$

where $S_{\min}$ denotes the minimum cross-sectional area of the hinge.

The aforementioned two stress equations give the relationships between the stiffness/compliance values and architecture parameters of the stage as follows:

$$\frac{wt}{K_{\text{in}}} \ge \frac{n_aQ}{\sigma_y} \quad (28a)$$

$$wtd_{22} \ge \frac{n_aQA_a}{\sigma_y} \quad (28b)$$

which provide another guideline for the design of the stage dimensions without the risk of plastic failures.

B. Dynamics Analysis

1) Dynamics Modeling: In order to fully describe the free vibrations of the XY stage, the independence of the secondary stages should be considered. Thus, six generalized coordinates are selected as

$$\mathbf{q} = [q_1 \;\; q_2 \;\; u_1 \;\; u_2 \;\; u_3 \;\; u_4]^T \tag{29}$$

which are sufficient, as elaborated in Fig. 7. The kinetic and potential energies ($T = \sum T_i$ and V) for the entire stage can be expressed in terms of the generalized coordinates only. For instance, the kinetic energy T_1 for limb 1 and the potential energy V for the entire stage are shown in Appendix A. Substituting the kinetic and potential energies into Lagrange's equation

$$\frac{d}{dt}\frac{\partial T}{\partial \dot{q}_i} - \frac{\partial T}{\partial q_i} + \frac{\partial V}{\partial q_i} = F_i \tag{30}$$

allows the generation of dynamics equation describing a free motion of the stage

$$\mathbf{M}\ddot{\mathbf{q}} + \mathbf{K}\mathbf{q} = \mathbf{0} \tag{31}$$

where the mass and stiffness matrices take on the forms

$$\mathbf{M} = \begin{bmatrix} M_{11} & 0 & 0 & M_{14} & 0 & M_{16} \\ 0 & M_{22} & M_{23} & 0 & M_{25} & 0 \\ 0 & M_{32} & M_{33} & 0 & 0 & 0 \\ M_{41} & 0 & 0 & M_{44} & 0 & 0 \\ 0 & M_{52} & 0 & 0 & M_{55} & 0 \\ M_{61} & 0 & 0 & 0 & 0 & M_{66} \end{bmatrix} \tag{32}$$

$$\mathbf{K} = \text{diag}\{K_{11} \;\; K_{22} \;\; K_{33} \;\; K_{44} \;\; K_{55} \;\; K_{66}\} \tag{33}$$

whose matrix factors are shown in Appendix B.

Based on the theory of vibrations, the mode equation can be derived as

$$(\mathbf{K} - \omega_j^2 \mathbf{M})\mathbf{\Phi}_j = \mathbf{0} \tag{34}$$

where the eigenvector $\mathbf{\Phi}_j$ (for $j = 1, 2, \ldots, 6$) represents a mode shape and eigenvalue ω_j^2 describes the corresponding natural cyclic frequency, which can be obtained by solving the characteristic equation

$$|\mathbf{K} - \omega_j^2 \mathbf{M}| = \mathbf{0}. \tag{35}$$

Then, the natural frequency can be computed as $f_j = (1/2\pi)\omega_j$.

TABLE III
NATURAL FREQUENCIES OF AN XY STAGE

Mode sequence	1	2	3	4	5	6
Matrix model	111.9	111.9	112.0	112.0	155.2	155.2
FEA (Hz)	101.4	101.6	101.8	112.2	135.6	135.7
Deviation (%)	10.4	10.1	10.0	–0.2	14.5	14.4

2) Model Verification With FEA: The dynamics equation for the evaluation of natural frequency of the XY stage is verified by the modal analysis via FEA undertaken with ANSYS. Although only the first natural frequency is mostly concerned for the design and control purposes, the frequencies of the first six modes are obtained and tabulated in Table III. Taking FEA results as the benchmark, one can observe that the established dynamics model overestimates the stage natural frequencies with deviations less than 15%.

Moreover, the mode shape vectors $\mathbf{\Phi}_j$ corresponding to natural cyclic frequencies ω_j are calculated as well. The elements of each vector describe the vibrational displacement magnitudes of the selected generalized coordinates (29), and hence, interpret a mode shape of the mechanism. The six vectors are assembled into a mode shape matrix, which is uniformed with respect to the mass matrix, and is shown as (36), at the bottom of this page.

Additionally, the first eight mode shapes extracted by ANSYS are illustrated in Fig. 12, where the first six ones are consistent with the mode shape matrix (36), and hence, validate the accuracy of the established dynamics model as well. Besides, it can be identified that the secondary stages (with coordinates u_1 to u_4) in the four limbs are the major sources of lowest frequency vibrations, as shown in Fig. 12(a)–(d). In addition, the two translational vibrations of the stage occur at the fifth and sixth modes, and the rotational vibration exhibits the seventh mode, as illustrated in Fig. 12(e)–(g), respectively. The vibrations of the secondary stages of four decouplers account for the eighth mode depicted by Fig. 12(h). Furthermore, it is observed that the rotational resonance frequency (310.3 Hz) is over twice higher than translational resonance frequencies (135.7 Hz). Therefore, the designed stage has only two translational motions since the parasitic rotation is substantially reduced. On the other hand, the resonance vibrations of the four limb secondary stages should be suppressed to widen the bandwidth of structure, which leads to one new direction for our further research works.

$$\begin{aligned} \mathbf{\Phi} &= [\mathbf{\Phi}_1 \; \mathbf{\Phi}_2 \; \mathbf{\Phi}_3 \; \mathbf{\Phi}_4 \; \mathbf{\Phi}_5 \; \mathbf{\Phi}_6] \\ &= \begin{bmatrix} 0.0123 & -0.0001 & 0.0000 & 0.0000 & -0.2446 & 0.0000 \\ 0.0001 & 0.0123 & 0.0000 & 0.0000 & 0.0000 & 0.2446 \\ 0.0211 & 3.5546 & -3.5339 & 0.4909 & 0.0000 & -0.3513 \\ 3.5546 & -0.0211 & 0.4909 & 3.5339 & 0.3513 & 0.0000 \\ 0.0211 & 3.5546 & 3.5339 & -0.4909 & 0.0000 & -0.3513 \\ 3.5546 & -0.0211 & -0.4909 & -3.5339 & 0.3513 & 0.0000 \end{bmatrix}. \end{aligned} \tag{36}$$

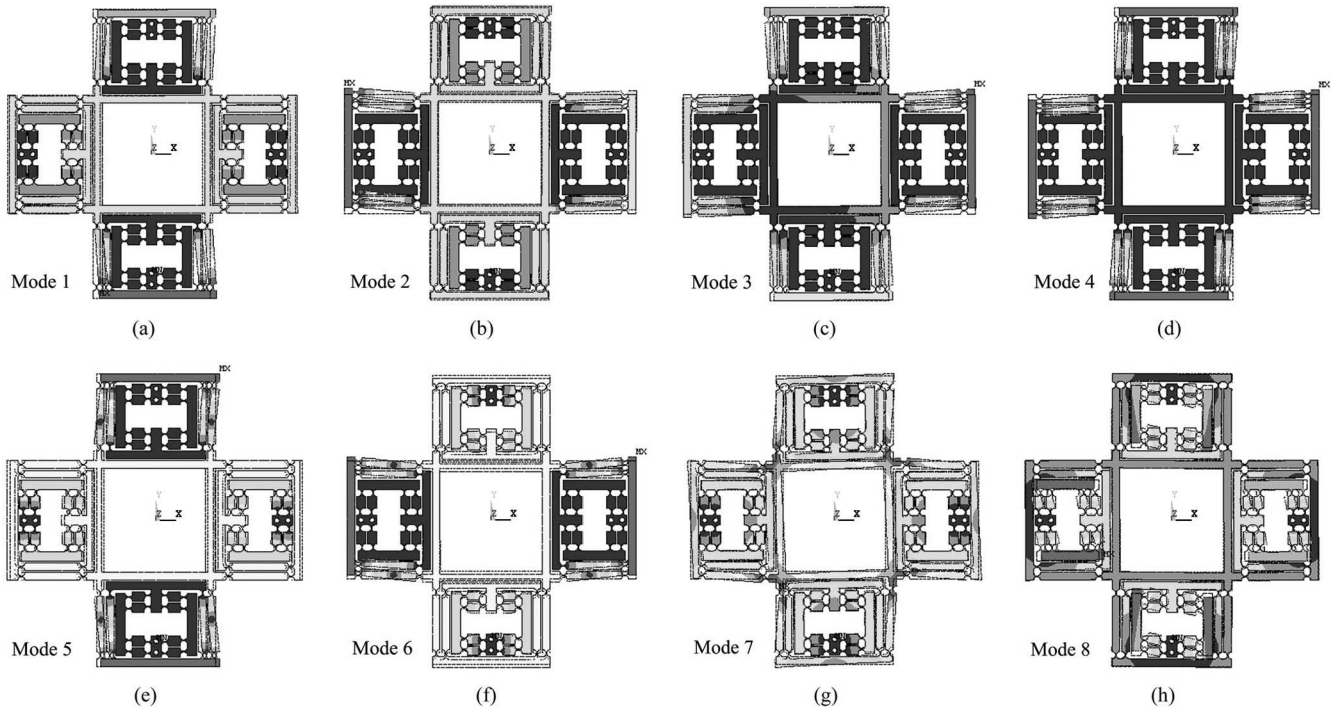

Fig. 12. First eight mode shapes of the XY stage obtained by ANSYS.

VI. Dimension Optimization of the XY Stage

In order to develop an XY micromanipulator for practical applications, it is a key step to determine its dimensions by simultaneously taking into account its performances. To increase the natural frequency of the stage, the mobile platform mass is reduced by removing unnecessary mass. The stroke of the two PZT is assigned as $20\,\mu$m. Additionally, the FEA results for the stage performances are taken as true values. Considering that the analytical models overestimate the stage performances with deviations around 15%, a compensation factor $\eta = 0.85$ is adopted in the optimization process to compensate for the derived models.

A. Optimization Statement

With the selection of natural frequency of the stage as an objective function, the optimization is stated as follows.

1) Maximize: Natural frequency (f).
2) Variables to be optimized: r, t, l_1, l_2, and l_8.
3) Subject to:
   a) amplification ratio $\eta A_s \geq 6$;
   b) input stiffness value $\eta K_{\rm in}/ \leq K_{\rm PZT}$;
   c) output compliance $\eta C_{\rm out}^{\theta z} \leq 0.5$ mrad/N·m;
   d) free of inelastic deflections guaranteed by (26) and (28) with a safety factor $n_a = 1.5$;
   e) parameter ranges: $2.5\,{\rm mm} \leq r \leq 6\,{\rm mm}$, $0.3\,{\rm mm} \leq t \leq 2\,{\rm mm}$, $5\,{\rm mm} \leq l_1 \leq 20\,{\rm mm}$, $1\,{\rm mm} \leq l_2 \leq 5\,{\rm mm}$, and $30\,{\rm mm} \leq l_8 \leq 100\,{\rm mm}$.

As far as a material with a specific thickness ($w = 12.7\,{\rm mm}$ in this research) is concerned, five parameters (r, t, l_1, l_2, and l_8) need to be optimized since other parameters can be designed by considering the length and width of the PZT with the addition of a proper assembling space. The amplification ratio of the stage is specified to guarantee a travel range not less than $120\,\mu$m for the mobile platform. The input stiffness should not exceed the minimum stiffness of the adopted PZT, i.e., $K_{\rm PZT} = 10\,{\rm N}/\mu{\rm m}$. And the output rotational compliance of the stage with respect to the z-axis $C_{\rm out}^{\theta z} = \mathbf{C}_B(6,6)$ is constrained to ensure the manipulation accuracy with external forces exerted. Meanwhile, the stage should be designed with the elimination of plastic failures for the safety reason. The upper bounds for design variables are all limited so as to generate a compact manipulator.

B. PSO and Results

The PSO is adopted in the current problem due to its superiority of performance over other methods such as direct search approach and genetic algorithm (GA) [41], [42].

The optimization is implemented with MATLAB via a PSO toolbox [43], and the optimized dimensions are: $r = 2.50$ mm, $t = 0.46$ mm, $l_1 = 10.87$ mm, $l_2 = 1.86$ mm, and $l_8 = 56.00$ mm (see Figs. 7–9), which leads to an XY stage with $A_s = 6.0$, $K_{in} = 10.0\,{\rm N}/\mu{\rm m}$, $C_{\rm out}^{\theta z} = 0.44\,{\rm mrad/N{\cdot}m}$, and $f = 115.6$ Hz, respectively.

VII. Performance Evaluation With FEA

A. Performance Test of the Optimized Stage

The performance of the optimized XY stage is tested by FEA with ANSYS software package. The simulation results exhibit that the stage has a workspace size around $124 \times 124\ \mu{\rm m}^2$ indicating an amplification ratio of 6.2. Besides, the input stiffness

is 9.9 N/μm, the rotational output compliance is 0.46 mrad/N·m, and the natural frequency is up to 110.2 Hz, which reveals the efficiency of the performed optimization. When the stage translates along the x-direction due to the actuation of PZT 1 with an input displacement $20\,\mu$m, the crosstalk of the mobile platform in the y-direction is 0.03% and the parasitic rotation around the z-axis is $0.9\,\mu$rad, which are all neglectable, and hence, indicate a well-decoupled motion of the stage. In addition, the maximal transverse displacement at the output end of decoupler 2 is less than $0.5\,\mu$m, i.e., less than 0.5% of axial displacement of the decoupler, which implies the well isolation property of the actuators. Furthermore, the nonlinear statics FEA results in a linear relationship between the input force and corresponding displacement, which means that there is no stress stiffening in the XY stage.

B. Misalignment Effect of Actuation Axis

As is observed that, instead of direct actuation, the proposed XY TDPS are driven by two PZT actuators through two decouplers to realize the actuation isolation. It is commonly assumed that the actuation axis of each PZT actuator is vertical to axial direction and parallel to lateral direction of the corresponding decoupler. Nevertheless, the actuation axis may be misaligned due to assembly errors of PZT in practice. In order to simulate this situation, the effects of misalignment of actuation axis on stage performances and decoupler lateral displacement are investigated via FEA. When the stage is driven by PZT 1 with a displacement of $20\,\mu$m along with different misaligned angles for the actuation axis, the FEA results are described in Table IV.

It can be observed that, with a misaligned angle of the actuation axis within 5°, the workspace size and displacement amplification ratio of the stage as well as lateral displacement of the corresponding decoupler are obviously influenced as expected. On the other hand, although the variation tendencies of cross-axis translation and parasitic rotation of the stage are not uniform along with the increase of the misalignment angle from 0° to 5°, the influences on these performances are still negligible, which are contributed by the proposed decoupler and XY TDPS mechanism with a mirror-symmetric architecture.

TABLE IV
INFLUENCE OF ACTUATION AXIS MISALIGNMENT ON STAGE PERFORMANCE

Misaligned angle	0°	3°	5°
Stage workspace (μm)	124.73	121.85	93.75
Stage amplification ratio	6.24	6.09	4.69
Stage cross-axis error (μm)	–0.05	–0.08	0.01
Stage parasitic rotation (μrad)	–0.20	–4.49	2.01
Decoupler lateral motion (μm)	0.00	4.11	2.19

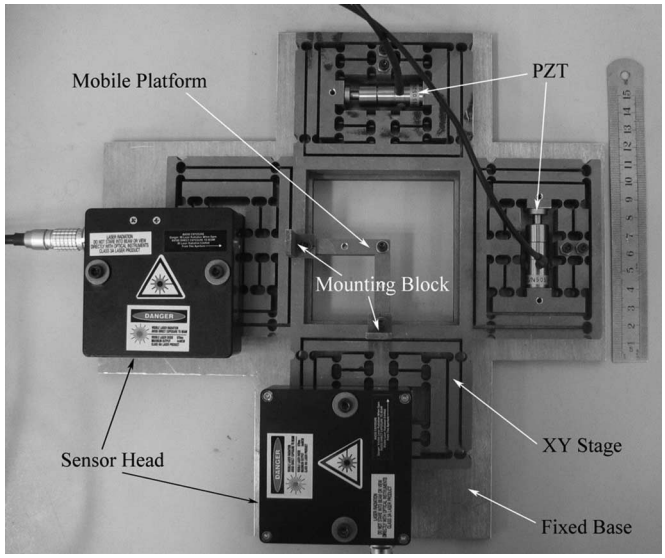

Fig. 13. Prototype of the totally decoupled XY parallel micromanipulator.

VIII. EXPERIMENTAL RESULTS AND DISCUSSIONS

A prototype of the XY micromanipulator designed with optimal parameters has been constructed, as shown in Fig. 13. The stage is fabricated through the wire electrical discharge machining (EDM) process from a piece of AL7075-T651 material, which has a higher strength, elasticity, and lighter mass than steel material. Two 20-μm stroke PZTs (PAS020 from Thorlabs, Inc.) are adopted to drive the XY stage, and the PZT is actuated with a voltage of 0–75 V. The two PZTs are inserted into the stage with interference fits; hence, no clearances exist between actuators and the stage, which allows a proper operation without adoption of preloading springs due to elastic deformations of the hinges. By mounting two blocks on the mobile platform that are considered as rigid bodies, the output motions of the stage are measured by two laser displacement sensors (Microtrak II head model: LTC-025-02 from MTI Instrument, Inc.) with a resolution of $0.04\,\mu$m and linearity better than 0.05% over a measuring range of 2 mm.

First, the parasitic rotation of the XY stage is tested. When the stage is driven to translate along the x-direction, the mobile platform displacement in the x-axis is monitored by two sensors that are mounted in parallel with a known distance. By this approach, it has been calculated that the parasitic rotation of the mobile platform is less than 1.3 mrad. Second, the motion range and cross-axis error of the manipulator in the two working directions are tested. When the XY stage is driven by one PZT to translate along the x (y) direction, the displacements in x- and y-axis are measured simultaneously to determine the motion range and crosstalk in two axes. The experiments have been conducted under the open-loop control. Fig. 14 plots the experimental results for the motion test along the two axes, where the hysteresis behavior is induced by the adopted PZT. It is observed that XY stage has a workspace around $117 \times 117\ \mu\text{m}^2$ with the maximum crosstalk of 1.5% between the two working axes and an amplification ratio of 5.85 for the XY stage. For the application of micro-/nanopositioning, the hysteresis effect can be reduced by designing a sophisticated feedforward or feedback controller.

The experimental results confirm the decoupling motion of the XY stage. The deviations in the experiment from the FEA results may arise from manufacturing tolerances of the stage and misalignment errors of PZT actuation axes. Although the output decoupling of the XY TDPS is enabled by employing compound

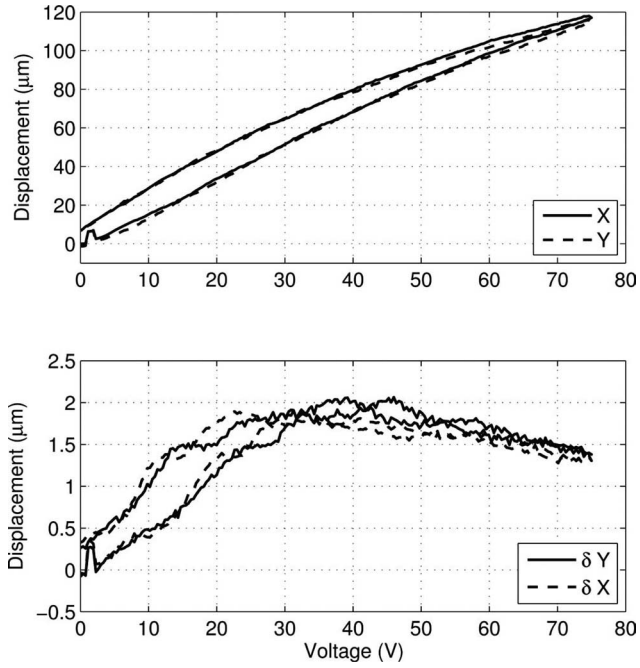

Fig. 14. Experimental results of motion ranges and cross-axis errors in the x and y-axis.

parallelogram flexures, the limitation of the mechanism comes from the compound flexures themselves. It is shown [44] that a transverse displacement for primary stage of a compound parallelogram flexure results in a loss of axial stiffness of the stage, and the relationship between the stiffness and the displacement is nonlinear in nature. Hence, the behavior of stage stiffness in x (or y) direction influenced by the actuation force of PZT 2 (or PZT 1) cannot be captured by the current research, since it is based on the matrix method characterizing a linear relationship only. In this sense, a nonlinear modeling is expected in the next research step to acquire an accurate model. Besides, as illustrated in [44], the axial stiffness reduction can be compensated by adopting compound parallelogram flexures with certain tilted angles of the four limbs. In our future work, the effects of titled flexures on stage performances will be investigated, and the out-of-plane performances of the XY stage will be studied as well.

IX. Conclusion

A conceptual design of a class of totally decoupled XY flexure parallel micromanipulator is proposed in this paper. The stage owns both input and output decoupling properties in virtue of actuation isolation and decoupled output motion, whose properties are attractive in micro-/nanoscale manipulation. A modified displacement amplifier with large transverse stiffness is used to amplify the PZT stroke and provide actuator bearing. The matrix-based method is applied in the kinematics and dynamics modeling of the XY stage, and validated by FEA via ANSYS. Based on PSO approach, the stage architecture optimization is carried out to achieve a maximal natural frequency under performance constraints on input stiffness, output compliance, and workspace size. An optimized stage prototype is fabricated for performance tests. Both FEA and experimental studies show that the well-decoupled stage has both negligible parasitic rotation and cross-axis coupling errors. In addition, the FEA results imply that the proposed mirror-symmetric stage along with decouplers can tolerate some degree of misalignment errors for the PZT actuation axis.

Although only the right circular hinge is used in this paper, any other types of flexure hinges can also be employed into the designed stage. Furthermore, this concept can be extended to the design of TDPS with other types of motions as well.

Appendix I

Kinetic energy T_1 for limb 1 and potential energy V for the entire stage

$$\begin{aligned}T_1 = {} & \frac{1}{2}(m_3+m_4)\dot{d}_1^2 + \frac{1}{2}(m_7)(\dot{x}^2+\dot{y}^2) + \frac{1}{2}(2m_1) \\ & \times\left[\left(\frac{\dot{d}_1}{2}\right)^2+\left(\frac{\dot{q}_1}{2}\right)^2\right] + 8\left(\frac{1}{2}\right)\left(\frac{m_2}{12}\right)l_1^2\dot{\theta}_1^2 + 4\left(\frac{m_2}{2}\right) \\ & \times\left[\left(\frac{\dot{q}_1}{4}\right)^2+\left(\frac{\dot{d}_1}{4}\right)^2\right] + 4\left(\frac{m_2}{2}\right)\left[\left(\frac{\dot{q}_1}{4}\right)^2+\left(\frac{3\dot{d}_1}{4}\right)^2\right] \\ & + \frac{1}{2}(m_6)\left[\dot{u}_1^2+\left(\frac{\dot{x}+\dot{d}_1}{2}\right)^2\right] \\ & + 2\left(\frac{m_5}{2}\right)\left[\left(\frac{\dot{d}_1}{2}+\frac{\dot{x}+\dot{d}_1}{4}\right)^2+\left(\frac{\dot{u}_1}{2}\right)^2\right] \\ & + 2\left(\frac{m_5}{2}\right)\left[\left(\frac{\dot{x}}{2}+\frac{\dot{x}+\dot{d}_1}{4}\right)^2+\left(\frac{\dot{y}+\dot{u}_1}{2}\right)^2\right] \\ & + 2\left(\frac{1}{2}\right)\left(\frac{m_5}{12}\right)(l_8^2)\left(\frac{\dot{u}_1}{l_8}\right)^2 \\ & + 2\left(\frac{1}{2}\right)\left(\frac{m_5}{12}\right)(l_8^2)\left(\frac{\dot{y}-\dot{u}_1}{l_8}\right)^2 \end{aligned} \tag{37}$$

$$\begin{aligned}V = {} & 8\left(\frac{1}{2}\right)K_r\left[\left(\frac{u_1}{l_8}\right)^2+\left(\frac{u_2}{l_8}\right)^2+\left(\frac{u_3}{l_8}\right)^2+\left(\frac{u_4}{l_8}\right)^2\right] \\ & + \frac{1}{2}(K_{\text{in}})(q_1^2+q_2^2)\end{aligned} \tag{38}$$

with $K_r = \Delta M_z/\Delta\theta_z$.

Appendix II

The factors for the mass and stiffness matrices of the XY stage

$$\begin{aligned}M_{11} = M_{22} = {} & m_1\left(2A_s^2+\frac{2A_s^2}{A_a^2}-2A_sA_a-\frac{2A_s}{A_a}+A_a^2+1\right) \\ & + m_2\left(10A_s^2+\frac{2}{3}DA_s^2+\frac{2A_s^2}{A_a^2}-10A_sA_a-\frac{2}{3}DA_sA_a\right.\end{aligned}$$

$$-\frac{2A_s}{A_a}+5A_a^2+\frac{1}{3}DA_a^2+1\Bigg)+(m_3+m_4)$$
$$\times(4A_s^2-4A_sA_a+2A_a^2)+m_5\left(\frac{5}{2}A_s^2-5A_sA_a+\frac{71}{6}A_a^2\right)$$
$$+m_6\left(\frac{5}{2}A_s^2-A_sA_a+\frac{1}{2}A_a^2\right)+4m_7A_s^2 \tag{39}$$

$$M_{14}=M_{41}=M_{16}=M_{61}=M_{23}=M_{32}=M_{25}=M_{52}=\frac{1}{3}A_sm_5 \tag{40}$$

$$M_{33}=M_{44}=M_{55}=M_{66}=\frac{4}{3}m_5+m_6 \tag{41}$$

$$K_{11}=K_{22}=K_{\text{in}} \tag{42}$$

$$K_{33}=K_{44}=K_{55}=K_{66}=\frac{8K_r}{l_8^2} \tag{43}$$

with $D=l_1^2/(l_1^2+l_2^2)$.

REFERENCES

[1] D. Kim, D. Y. Lee, and D. G. Gweon, "A new nano-accuracy AFM system for minimizing Abbe errors and the evaluation of its measuring uncertainty," *Ultramicroscopy*, vol. 107, no. 4–5, pp. 322–328, 2007.

[2] E. Pernette, S. Henein, I. Magnani, and R. Clavel, "Design of parallel robots in microrobotics," *Robotica*, vol. 15, no. 4, pp. 417–420, 1997.

[3] Y.-M. Moon and S. Kota, "Design of compliant parallel kinematic machines," in *Proc. ASME Des. Eng. Tech. Conf. Comput. Inf. Eng. Conf.*, Montreal, QC, Canada, 2002, pp. 35–41.

[4] M. L. Culpepper and G. Anderson, "Design of a low-cost nano-manipulator which utilizes a monolithic, spatial compliant mechanism," *Precis. Eng.*, vol. 28, no. 4, pp. 469–482, 2004.

[5] B. H. Kang, J. T.-Y. Wen, N. G. Dagalakis, and J. J. Gorman, "Analysis and design of parallel mechanisms with flexure joints," *IEEE Trans. Robot.*, vol. 21, no. 6, pp. 1179–1185, Dec. 2005.

[6] W. J. Chen, W. Lin, K. H. Low, and G. Yang, "A 3-DOF flexure-based fixture for passive assembly of optical switches," in *Proc. IEEE/ASME Int. Conf. Adv. Intell. Mechatronics*, Monterey, CA, 2005, pp. 618–623.

[7] X. Tang and I.-M. Chen, "A large-displacement and decoupled XYZ flexure parallel mechanism for micromanipulation," in *Proc. IEEE Int. Conf. Autom. Sci. Eng.*, Shanghai, China, 2006, pp. 75–80.

[8] P. R. Ouyang, R. C. Tjiptoprodjo, W. J. Zhang, and G. S. Yang, "Micro-motion devices technology: The state of arts review," *Int. J. Adv. Manuf. Technol.*, vol. 38, no. 5–6, pp. 463–478, 2008.

[9] S. T. Smith, *Flexures: Elements of Elastic Mechanisms*. Boca Raton, FL: CRC Press, 2000.

[10] J. Angeles, *Fundamentals of Robotic Mechanical Systems: Theory, Methods, and Algorithms*, 2nd ed. New York: Springer-Verlag, 1997.

[11] J.-P. Merlet, *Parallel Robots*. London, U.K.: Kluwer, 2000.

[12] D. Zhang, C. Chang, T. Ono, and M. Esashi, "A piezodriven XY-microstage for multiprobe nanorecording," *Sens. Actuators A, Phys.*, vol. 108, no. 1, pp. 230–233, 2003.

[13] Y. Lu, C. K. Pang, J. Chen, H. Zhu, J. P. Yang, J. Q. Mou, G. X. Guo, B. M. Chen, and T. H. Lee, "Design, fabrication and control of a micro X–Y stage with large ultra-thin film recoding media platform," in *Proc. IEEE/ASME Int. Conf. Adv. Intell. Mechatronics*, Monterey, CA, 2005, pp. 19–24.

[14] K.-B. Choi and D.-H. Kim, "Monolithic parallel linear compliant mechanism for two axes ultraprecision linear motion," *Rev. Sci. Instrum.*, vol. 77, no. 6, pp. 065106-1–065106-7, 2006.

[15] Y. Li and Q. Xu, "A novel design and analysis of a 2-DOF compliant parallel micromanipulator for nanomanipulation," *IEEE Trans. Autom. Sci. Eng.*, vol. 3, no. 3, pp. 248–254, Jul. 2006.

[16] Q. Yao, J. Dong, and P. Ferreira, "Design, analysis, fabrication and testing of a parallel-kinematic micropositioning XY stage," *Int. J. Mach. Tools Manuf.*, vol. 47, no. 6, pp. 946–961, 2007.

[17] K.-B. Choi and J. J. Lee, "Ultra-precision stage with linear parallel compliant mechanism using 4-PP flexural joints," in *Proc. 11th Int. Conf. Mechatronics Technol.*, Ulsan, Korea, 2003, pp. 53–56.

[18] K.-B. Choi and J. J. Lee, "Analysis and design of linear parallel compliant stage for ultra-precision motion based on 4-PP flexural joint mechanism," in *Proc. Int. Conf. Smart Manuf. Appl.*, Gyeonggi-do, Korea, 2008, pp. 35–38.

[19] J. Ryu, S.-S. Kim, and S.-S. Kim, "A criterion on inclusion of stress stiffening effects in flexible multibody dynamic system simulation," *Comput. Struct.*, vol. 62, no. 6, pp. 1035–1048, 1997.

[20] Q. Xu and Y. Li, "Structure improvement of an XY flexure micromanipulator for micro/nano scale manipulation," in *Proc. 17th IFAC World Congr.*, Seoul, Korea, 2008, pp. 12733–12738.

[21] S. Awtar and A. H. Slocum, "Design of parallel kinematic XY flexure mechanisms," in *Proc. ASME Des. Eng. Tech. Conf. Comput. Inf. Eng. Conf.*, Long Beach, CA, 2005, pp. 89–99.

[22] H. Wang and X. Zhang, "Input coupling analysis and optimal design of a 3-DOF compliant micro-positioning stage," *Mech. Mach. Theory*, vol. 43, no. 4, pp. 400–410, 2008.

[23] S. Awtar. (2004, Feb.) Synthesis and analysis of parallel kinematic XY flexure mechanisms, Ph.D. dissertation, Massachusetts Inst. Technol. (MIT), Cambridge [Online]. Available: http://web.mit.edu/~shorya/www/PHD/Thesis/.

[24] I. A. Bonev, D. Zlatanov, and C. M. Gosselin, "Singularity analysis of 3-DOF planar parallel mechanisms via screw theory," *ASME J. Mech. Des.*, vol. 125, no. 3, pp. 573–581, 2003.

[25] X. Kong and C. M. Gosselin, "Type synthesis of 3-DOF translational parallel manipulators based on screw theory," *ASME J. Mech. Des.*, vol. 126, no. 1, pp. 83–92, 2004.

[26] J. M. Hervé, "Uncoupled actuation of pan-tilt wrists," *IEEE Trans. Robot.*, vol. 22, no. 1, pp. 56–64, Feb. 2006.

[27] J. Meng, G. Liu, and Z. Li, "A geometric theory for analysis and synthesis of sub-6 DoF parallel manipulators," *IEEE Trans. Robot.*, vol. 23, no. 4, pp. 625–649, Aug. 2007.

[28] X.-J. Liu and J. Wang, "A new methodology for optimal kinematic design of parallel mechanisms," *Mech. Mach. Theory*, vol. 42, no. 9, pp. 1210–1224, 2007.

[29] D. Chablat and P. Wenger, "A new concept of modular parallel mechanism for machining applications," in *Proc. IEEE Int. Conf. Robot. Autom.*, Taipei, Taiwan, 2003, pp. 3965–3970.

[30] N. Lobontiu and E. Garcia, "Analytical model of displacement amplification and stiffness optimization for a class of flexure-based compliant mechanisms," *Comput. Struct.*, vol. 81, no. 32, pp. 2797–2810, 2003.

[31] J. H. Kim, S. H. Kim, and Y. K. Kwak, "Development and optimization of 3-D bridge-type hinge mechanisms," *Sens. Actuators A, Phys.*, vol. 116, no. 3, pp. 530–538, 2004.

[32] B.-J. Yi, G. Chung, H. Na, W. Kim, and I. Suh, "Design and experiment of a 3-DOF parallel micromechanism utilizing flexure hinges," *IEEE Trans. Robot. Autom.*, vol. 19, no. 4, pp. 604–612, Aug. 2003.

[33] L. L. Howell, *Compliant Mechanisms*. New York: Wiley, 2001.

[34] Y. Koseki, T. Tanikawa, N. Koyachi, and T. Arai, "Kinematic analysis of translational 3-DOF micro parallel mechanism using matrix method," in *Proc. IEEE/RSJ Int. Conf. Intell. Robots Syst.*, Takamatsu, Japan, 2000, pp. 786–792.

[35] L. C. Hale and A. H. Slocum, "Optimal design techniques for kinematic couplings," *Precis. Eng.*, vol. 25, no. 2, pp. 114–127, 2001.

[36] H.-H. Pham and I.-M. Chen, "Stiffness modeling of flexure parallel mechanism," *Precis. Eng.*, vol. 29, no. 4, pp. 467–478, 2005.

[37] J. S. Dai and X. Ding, "Compliance analysis of a three-legged rigidly-connected platform device," *ASME J. Mech. Des.*, vol. 128, no. 4, pp. 755–764, 2006.

[38] Y. K. Yong, T.-F. Lu, and D. C. Handley, "Review of circular flexure hinge design equations and derivation of empirical formulations," *Precis. Eng.*, vol. 32, no. 2, pp. 63–70, 2008.

[39] L. C. Hale. (1999, Feb.) Principles and techniques for designing precision machines, Ph.D. dissertation, Massachusetts Inst. Technol. (MIT), Cambridge [Online]. Available: http://e-reports-ext.llnl.gov/pdf/235415.pdf

[40] K.-B. Choi and J. J. Lee, "Static model for flexure-based compliant mechanism driven by piezo stacks," *Proc. Inst. Mech. Eng. Part C-J. Mech. Eng. Sci.*, vol. 222, no. 4, pp. 703–709, 2008.

[41] M. Clerc and J. Kennedy, "The particle swarm-explosion, stability, and convergence in a multidimensional complex space," *IEEE Trans. Evol. Comput.*, vol. 6, no. 1, pp. 58–73, Feb. 2002.

[42] Q. Xu and Y. Li, "Error analysis and optimal design of a class of translational parallel kinematic machine using particle swarm optimization," *Robotica*, vol. 27, no. 1, pp. 67–78, 2009.

[43] B. Birge, "PSOt—A particle swarm optimization toolbox for use with MATLAB," in *Proc. IEEE Swarm Intell. Symp.*, Indianapolis, IN, 2003, pp. 182–186.
[44] S. Awtar and A. H. Slocum, "Closed-form nonlinear analysis of beam-based flexure modules," in *Proc. ASME Des. Eng. Tech. Conf. Comput. Inf. Eng. Conf.*, Long Beach, CA, 2005, pp. 101–110.

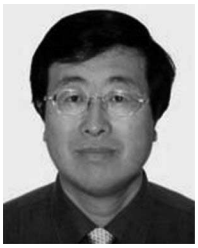

Yangmin Li (M'98–SM'00) received the B.S. and M.S. degrees from Jilin University, Changchun, China, in 1985 and 1988, respectively, and the Ph.D. degree from Tianjin University, Tianjin, China, in 1994, all in mechanical engineering.

He is currently a Professor of electromechanical engineering at the University of Macau, Macao, China, where he also directs the Mechatronics Laboratory. He has authored or coauthored about 190 scientific papers. He is a council member and an Editor of the *Chinese Journal of Mechanical Engineering*. He is also a member of the Editorial Boards of the *International Journal of Control, Automation, and Systems*, *International Journal of Advanced Robotic Systems*, *Frontiers of Mechanical Engineering in China*, *Journal of Robotics*, etc. His current research interests include micro-/nanomanipulation, nanorobotics, micromanipulator, mobile robot, modular robot, and multibody dynamics and control.

Prof. Li is a Technical Editor of the IEEE/ASME TRANSACTIONS ON MECHATRONICS. He is a member of the American Society of Mechanical Engineers (ASME). He has been a member of about 70 international conference program committees.

Qingsong Xu received the B.S. degree in mechatronics engineering (Hons.) from Beijing Institute of Technology, Beijing, China, in 2002, and the M.S. and Ph.D. degrees in electromechanical engineering from the University of Macau, Macao, China, in 2004 and 2008, respectively.

He is currently a Postdoctoral Fellow at the University of Macau. His current research interests include mechanism design, kinematics, dynamics, and control of parallel robots, micro-/nanorobots, and mobile robots with various applications.